Indian Journal of Chemical Technology
Vol. 29, September 2022, pp. 540-546
DOI: 10.56042/ijct.v29i5.62576

# NiO nanoparticles via calcination of a Schiff base complex: Photocatalytic and microbicidal activity

Ayşegül Şenocak*[,1] & Rızvan İmamoğlu[2]

[1]Department of Chemistry, Faculty of Art and Science, University of Tokat Gaziosmanpaşa, 60240, Turkey

[2]Department of Molecular Biology and Genetics, Faculty of Science, University of Bartın, 74100, Turkey

E-mail: aysegul.senocak@gop.edu.tr, ayseon@gmail.com

*Received 25 April 2022; accepted 19 July 2022*

Calcination method has been used to create NiO nanoparticles with a diameter of 19 to 30 nm from [NiL] [L: 2,2'-((1E,1'E)-(1,2-phenylenebis(azanylylidene))bis(methanylylidene))bis(4-bromophenolate)]. Formation and purity of the NiO nanoparticles produced under mild conditions without any special needs are evidenced by fourier-transformed infrared (FT-IR) spectroscopy, ultraviolet visible (UV-Vis) spectroscopy, X-ray powder diffraction (XRD), energy-dispersive X-ray (EDX) spectroscopy and scanning transmission electron microscopy (STEM). According to the spectral methods, transformation of the synthesized nickel-Schiff base complex into the nanoparticles has been achieved with high purity, high crystallinity and low agglomeration by thermal decomposition which is an efficient and simple approach. The nanoparticles are employed as a catalyst for the decomposition of methylene blue, an industrial synthetic dye, and the nanoparticles exhibit mild photocatalytic activity. Furthermore, biological activity of nanoparticles has been investigated on five bacterial strains and two fungi, with promising results.

**Keywords:** Biological Activity, Calcination, Catalytic Activity, Industrial dyes, NiO nanoparticles

Nanomaterials (NPs), defined as tiny particles ranging in size from 1 and 100 nanometers, have sparked a lot of interest and have been widely explored with the goal of developing compounds with unimagined characteristics in comparison to regular materials. Transition metal oxide NPs, in particular, have propelled to prominence due to their usage in solar cells, sensor technology, liquid crystals and other fields[1]. NiO NPs as one of the metal oxide NPs subjected to a lot of interest have a wide variety of applications like alkaline batteries[2,3], solar cells[4,5], sensors[6,7], catalysis[8,9], and so on. Furthermore, several investigations have shown that NiO NPs have cytotoxic and antibacterial properties[10–13]. For the production of versatile NiO NPs with a diversified amount of applications, various synthetic approaches have been proposed, including solvothermal[14,15], hydrothermal[16,17], chemical precipitation[18], microemulsion[19,20], solid state thermal decomposition (calcination)[21,22], microwave assisted[23,24], sol-gel[25,26] and so on. Advantages such as low energy consumption and cost, being simple, high purity and yield, particle size adjustment have made calcination a highly favored process for NiO NPs production among the approaches described[27]. Due to these benefits, the approach has been employed to obtain NPs in many studies. In some of these studies, the complexes prepared with polydentate ligands, usually Schiff bases, were subjected to thermal decomposition to obtain targeted NiO NPs[28–34]. The resulting NiO NPs exhibited sizes ranging from 15-20 nm to 40-70 nm, depending on the working temperature. Dehno used an asymmetric Schiff base complex to produce NiO NPs with an approximate particle size of 55 nm[34]. Khalaji and Das reported that the NiO NPs calcined from two symmetrical Schiff base complexes had 10-15 nm particle size[30]. In the rest of the studies, complex structures prepared from commercially available small molecules like ammonia and ethylenediamine were calcined for NiO NPs, with 15 nm particle size[35–37].

Synthetic dyes are the most important water pollutants released by today's developing sectors like textile, leather, paper, food processing, and ceramics. More than 100,000 different types of dye are known to be in use, with around 15% of them ending up as waste in natural water springs[38]. The pollution created by industrial dyes like methylene blue, methyl red, alizarin yellow...etc. harmed the organisms in the water by forming a layer between them and sunlight. Besides, farming activities utilizing from this contaminated water have been directly affected public health negatively.

These synthetic dyes, which are referred to azo dyes because they include one or more azo groups (-N=N-), are non-biodegrable due to their aromatic stability. As a result, many effective remediation methods for synthetic dyes like coagulation, flocculation, reverse osmosis, membrane filtration and degradation have been developed[39]. Among these wastewater remediation approaches, photocatalytic degradation stands out as a green technology due to the use of directly solar energy[40]. Due to their versatility, nanoscale metals and their oxides have been considered effective photocatalysts for decomposition of synthetic dyes under various conditions[40–43].

In the light of the information given above, NiO NPs were prepared by calcination from a pioneer Schiff base complex without the need of any special equipment, surfactant or stabilizing agent. The NPs were characterized by FT-IR, UV-Vis, XRD, EDX and STEM methods. The as-synthesized NiO NPs were employed as a catalyst for photodegradation of methylene blue (MB) and decomposition kinetics were examined. The NiO NPs were also tested for antibacterial activity against gram-negative (*Escherichia coli*, *Pseudomonas aeruginosa* and *Klebsiella pneumonia*) and gram-positive (*Staphylococcus aureus* and *Enterococcus faecalis*) bacterial strains, and fungi (*Candida albicans* and *Calatheautilis*).

## Experimental Section

Commercially available o-phenylenediamine, 5-bromosalicylaldehyde, nickel(II) acetate tetrahydrate, p-toluenesulfonic acid, ethanol, and methanol were used without additional purification. FT-IR spectra were collected using a Jasco FT-IR 4700 spectrometer (400-4000 cm$^{-1}$). A Perkin-Elmer Lambda-35 UV-Vis spectrophotometer with a wavelength range of 200-800 nm was used to measure the electronic spectra of the NPs in ethanol solvent (10$^{-3}$ M). The Elementar Vario Micro Cube elemental analyzer was utilized to record the C, H, and N percentages of the compounds. XRD pattern was measured by a RIGAKU SmartLab X-ray diffractometer (XRD) with Cu Kβ radiation and assigned using the PDF2-Diffraction Database. Morphological features of the sample were studied by using a field emission gun TESCAN™ MAIA3 XMU scanning electron microscope (STEM).

### Preparation of the pioneer complex

The Schiff base and the nickel complex were prepared in accordance with the published method with minor changes[44]. At room temperature, 5-bromosalicylaldehyde (2 mmol, 402 mg) was reacted with o-phenylenediamine (1 mmol, 108 mg) as p-toluenesulfonic acid catalyzed. The light orange product immediately precipitating was isolated and washed with cold methanol. Anal. Calc. for $C_{20}H_{14}Br_2N_2O_2$ (%): C, 50.66; H, 2.98; N, 5.91 Found (%): C, 50.42; H, 3.07; N, 5.75. FT-IR (cm$^{-1}$): 3074, 3047 (C-H), 1613 (C=N), 1184 (C-O), 625 (C-Br). $^{1}$H NMR (d-DMSO, ppm): 12.93 (s, 2H, -OH), 8.93 (s, 2H, -CH=N-), 7.90 (d, 2H, -CH aromatic), 7.56 (dd, 2H, -CH aromatic), 7.45 (m, 4H, -CH aromatic), 6.96 (d, 2H, -CH aromatic). $^{13}$C NMR (d-DMSO, ppm): 162.67, 159.95, 142.50, 136.13, 134.24, 128.59, 121.93, 120.13, 119.63, 110.36.

By mixing Schiff base and nickel acetate solutions (1:1 ratio) prepared in methanol, the target complex was observed in the form of red precipitate, immediately. After stirring for several hours, the solution was isolated, washed with cold methanol and dried in air. Anal. Calc. for $C_{20}H_{12}Br_2N_2NiO_2$ (%): C, 45.25; H, 2.28; N, 5.28 Found (%): C, 45.39; H, 2.06; N, 5.47. FT-IR (cm$^{-1}$): 3059, 3027 (C-H), 1604 (C=N), 1188 (C-O), 649 (C-Br), 449 (Ni-N), 417 (Ni-O).

### Synthesis of the NiONPs

With the aim of preparation the NPs, the nickel Schiff base complex in a porcelain crucible was placed in an electrical oven programmed to 600°C. The green material obtained from calcination for 4 hours in the ambient atmosphere was washed with hot water and ethanol to get rid of any residue. The decomposition product dried in air was employed for characterization stages and activation studies.

### Decolorizing study of MB over the NiO NPs

The catalytic activity of the NiO NPs was tested for the decomposition of 10 ppm MB solution (in water) under sunlight. After addition of 20 mg NiO NPs to the MB solution (50 mL), it was stirred at room temperature in the dark for 30 min to set the equilibrium. After that, the reaction mixture was exposed to sunlight and samples were gathered every hour. The UV spectra of the centrifuged samples for 2 min were measured and % degradation was calculated based on the reduction of the main peak of MB at 665 nm (Eq. 1):

$$\%\,Degradation = \frac{(C_0 - C_t)}{C_0} x100 = \frac{(A_0 - A_t)}{A_0} x100 \ldots (1)$$

### Biological activities of the NiO NPs

The antibacterial activity of the NPs was investigated using the Broth Micro-dilution Assay with certain modifications[45,46]. For this purpose, gram-negative bacterial (*K. pneumonia*, *P. aeruginosa*, and *E.coli*), gram-positive bacterial (*E. faecalis* and *S. aureus*), and fungal strains (*C. albicans* and *C. utilis*), obtained from frozen stocks and kept at 37ºC for 24 h, were used to test the antimicrobial activity of the produced NiO NPs. Then, new cultures were prepared until 0.5 McFarland Unit at 37ºC. Negative controls were prepared using LB without bacteria. Absorbances of microtiter plates were read at 600 nm using a micro-plate reader (ThermoMultiscan) before ($0^{th}$ h) and after ($24^{th}$ h) the incubation at 37ºC. The percentage of compound-treated bacterial groups compared to the positive control was used to determine bacterial viability (bacterial viability of positive control was taken as 100 percent). The minimum inhibitory concentrations (MICs) were calculated by plotting the NPs concentration against the relative bacterial growth rate.

#### Statistical analysis

To assess statistical studies and related data sets, the Graph Pad Prism 8.0.2 tool was employed. To evaluate statistical significance, a probability value of $p < 0.05$ was utilized.

## Results and Discussion

The structural analysis of the NiO NPs produced by calcination of the Schiff base complex was carried out by FT-IR, UV-Vis, XRD, EDX and STEM spectroscopic methods. FT-IR spectroscopy is a practical tool for both characterization of NPs and detection of any possible organic residues remaining on NPs after calcination. For this reason, FT-IR spectra of the pioneer nickel complex and the NPs were measured and depicted in Fig. 1. Also, the important vibration peaks were listed in the experimental section. The nickel complex formation was revealed by the shift of C=N vibration peak from 1613 to 1604 $cm^{-1}$,the disappearance of the O-H stretching vibrations, and also the appearance of Ni-O and Ni-N vibration peaks. When it comes to the spectrum of NiO NPs, the Ni-O band observed at 417 $cm^{-1}$ pointed out the formation of the NPs, clearly[30,34,47]. Besides, not observing any other peak except for the one at the fingerprint region in the spectrum pointed out pure NP formation without any organic residue.

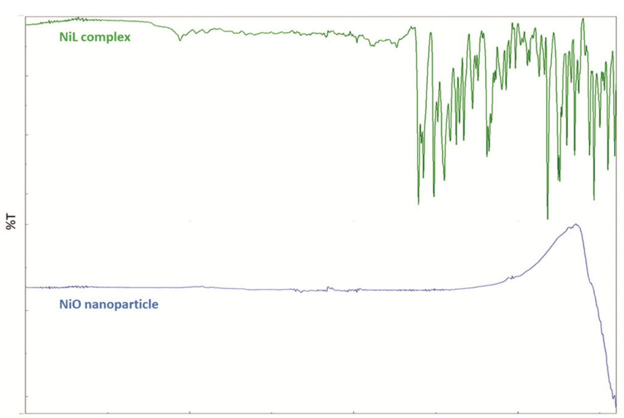


Fig. 1 ― FT-IR spectra of the synthesized materials

The electronic spectrum of the produced NPs was measured with intent to study the optical properties as displayed in Fig. 2. The strong band at 278 nm was attributed to NiO NPs in line with the literature[48–51]. There were no absorption bands in the visible region pointing out any impurities. Besides, there is a small band gap between the valence and the conduction bands in the NiO semiconductors and the electron motion in this band gap resulted in strong UV light absorption at 278 nm for the as synthesized NiO NPs. By using this transition, the optical band gap ($E_g$) was estimated on the basis of the equation $(Ah\upsilon)^2 = B\,(h\upsilon\text{-}E_g)$, where A and B are constants and hυ is the photon energy. By the extrapolation of the graph to the zero point of the inset of Fig 2, $E_g$ was calculated as 3.85 eV. This result pointed out a red shift in contrast to a blue shift that is generally observed for nanomaterials. This phenomena might be induced by the chemical defects or vacancies in the crystal which would cause lowering the band gap energy[52].

XRD pattern of the NPs synthesized in this study was depicted in Fig .3. The diffractive peak group at 37.25, 43.29, 62.89, 75.40 and 79.54 was an evidence for NiO

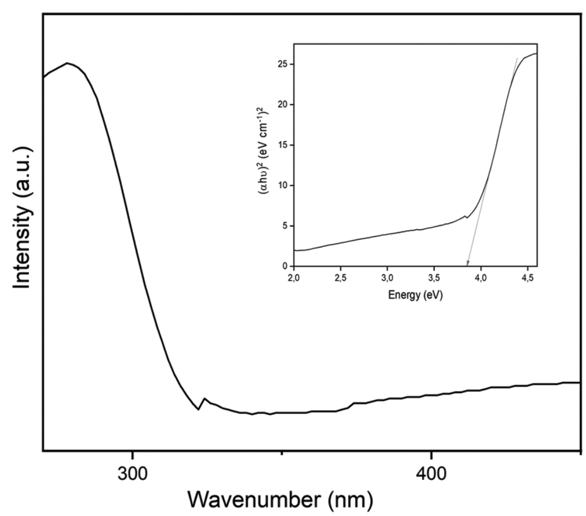


Fig. 2 ― Electronic spectrum and $(Ah\upsilon)^2$-hυ graph (inset) of the NiO NPs dispersed in ethanol formation while metallic Ni presence with weak intensity showed up at 44.50 by referring to absence of any other impurities. Moreover, the XRD results pointed out the presence of hexagonal NiO NPs with R-3m space group and lattice parameters of a=b=2.952 c=7.235 (DB Card No 00-022-1189), along with cubic Ni NPs with R-3m space group and lattice parameter of a=3.522 (DB Card No 01-077-8341). The XRD spectrum exhibiting sharp and high intensity peaks

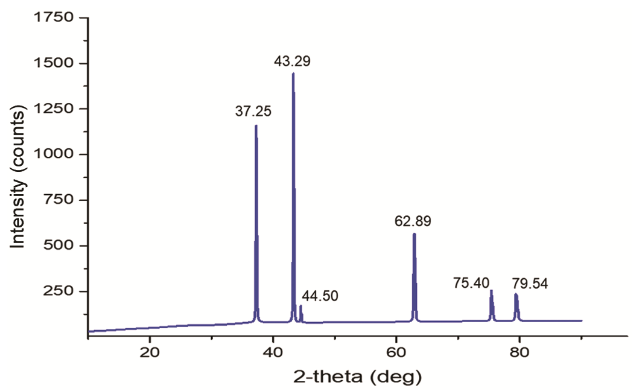


Fig. 3 ─ XRD pattern of the NiO NPs

proved formation of the well crystallized NiO NPs, and complete transformation of the complex molecules to the corresponding NPs at 600°C. The average size of prepared NPs was calculated based on the main diffraction peak at 43.29 by using the Scherrer formula (Eq 2.),

$$D_c = {}^{(K.\lambda)}\!\big/_{(\beta.cos\theta)} \qquad \dots (2)$$

where $D_c$ average size for the NPs, K constant (0.9), λ wavelength of CuKβ, β full width at half max of the main diffraction peak, θ Bragg's angle. Particle size of the NiO NPs calculated as 39.24 nm from XRD data was in accordance with the STEM measurements, approximately.

The morphology and particle size of the NiO NPs were studied by STEM. The STEM micrographs clearly indicated that spherical NiO NPs agglomerated to some extent (Fig. 4). In addition, NiO NPs exhibited non-uniform particle size ranging from 19 to 30 nm. EDX spectrum of the produced NPs proved the formation of the Ni and the NiO NPs without any impurity (Fig. 5).

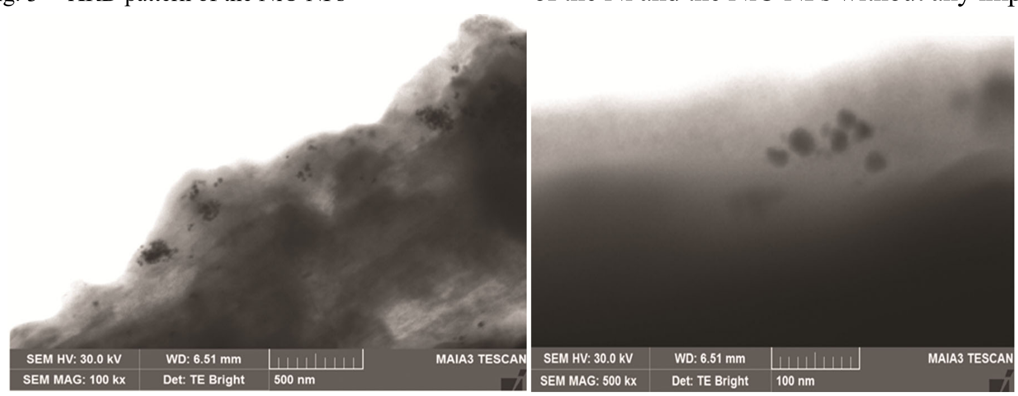


Fig. 4 ─ STEM micrographs of the NiO NPs

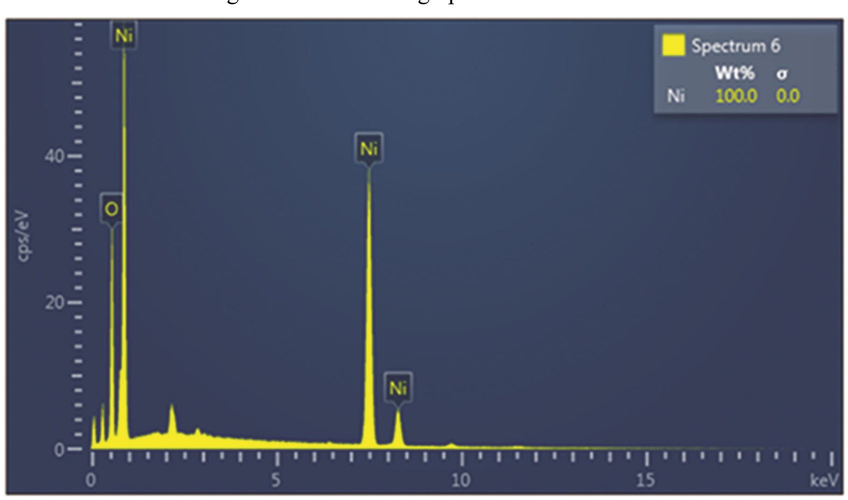


Fig. 5 ─ EDX image of the NiO NPs

Under sunlight, the catalytic effect of the produced NiO NPs on MB decomposition, an industrial dye that pollutes water supplies, was investigated. The addition of the NiO NPs to the MB solution as a catalyst resulted in 49.31% degradation, over the course of 9 h (Fig. 6). This finding highlighted the NiO NPs' modest photocatalytic effectiveness. The catalytic activity of the synthesized NPs may be attributed to electron transfer between the valence and the conduction bands as a consequence of exposure to sunlight, as well as the electrons and cavities formed on the NPs surface as a result of this transfer. The radicals, created by water molecules with these holes and electrons, react with the dye molecules, causing them to decompose into $CO_2$ and $H_2O$[58]. The pseudo-first-order decomposition kinetics for MB was examined using Eq. 3 where $C_0$ is the initial concentration and $C_t$ is the concentration at time t for MB. The rate constant for the studied decomposition reaction of MB was obtained as 0.0012 $min^{-1}$ ($R^2$= 0.986) (Fig. 7).

$$ln \, {}^{C_t}/_{C_0} = -k.t \qquad \dots (3)$$

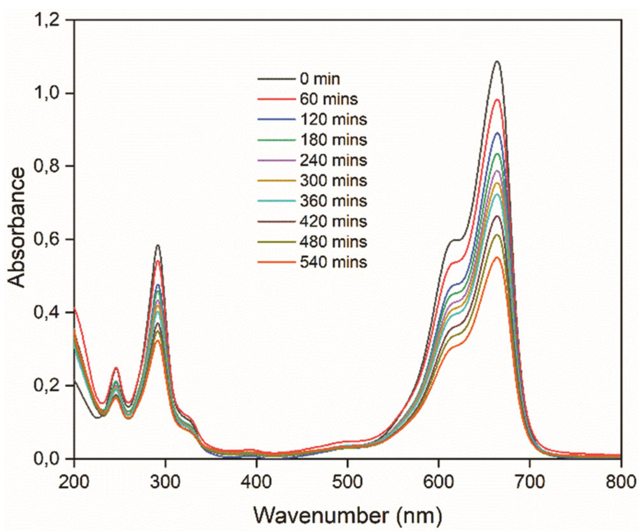


Fig. 6 — The NiO catalyzed photocatalytic degradation of MB over time

In this contribution, anti-bacterial effect of the prepared NPs were examined, too. According to the MIC data in Table 1, the NiO NPs have shown a good inhibition effect on both gram-negative (*E. coli*, *P. aeruginosa* and *K. pneumonia*) and gram-positive (*S. aureus* and *E. faecalis*) bacterial strains by comparison with the former studies[59–61]. Besides, NiO NPs showed a dose-dependent inhibitory effect on *C. albicans* and *C. utilis* fungi (Fig. 8). According to the MIC values, *K. pneumoniae* and *E.coli* were the most susceptible microorganisms against to the NiO nanoparticles. The least susceptible strains, on the other hand, were determined as *S. aureus* and *P. aeruginosa*. Even if the effect of nanoparticles on bacteria is not fully understood yet, this strong antibacterial activity might be resulted from the high tendency of the NiO NPs for penetrating to bacteria cells due to the reduction in their size. As a result of entering cell structure, NPs increase the permeability

Table 1 — Minimum inhibitory concentrations of NiO NPs

| Microorganisms | MIC Values of the NiO NPs(mg/mL) |
|---|---|
| *S. aureus* | 0.518±0.081 |
| *P. aeruginosa* | 0.538±0.082 |
| *K. pneumoniae* | 0.255±0.064 |
| *E. coli* | 0.239±0.058 |
| *E. faecalis* | 0.354±0.081 |
| *C. albicans* | 0.410±0.077 |
| *C. utilis* | 0.473±0.096 |

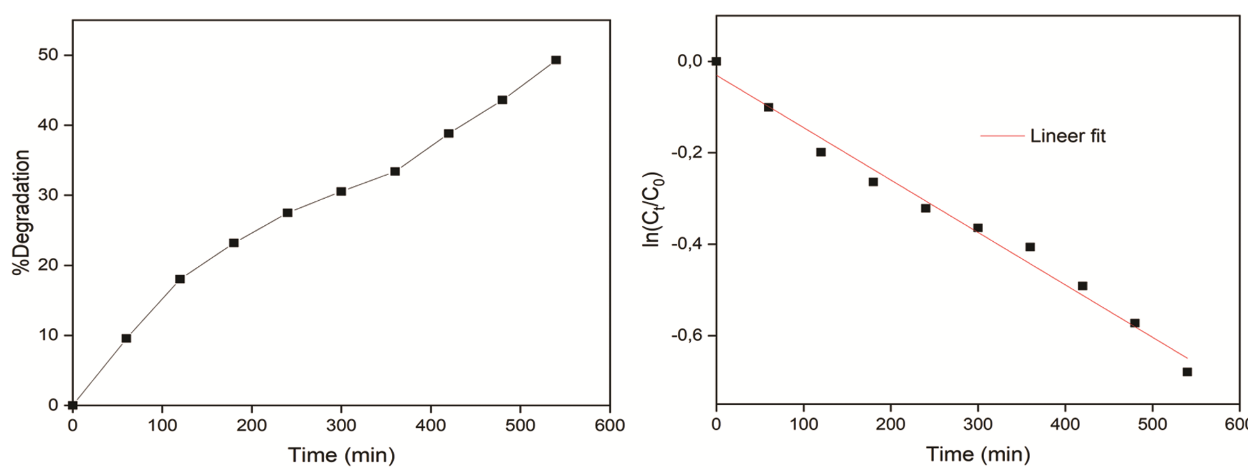


Fig. 7 (a) — Percentage degradation of MB over NiO NPs and (b) Pseudo-first-order kinetics for the decomposition

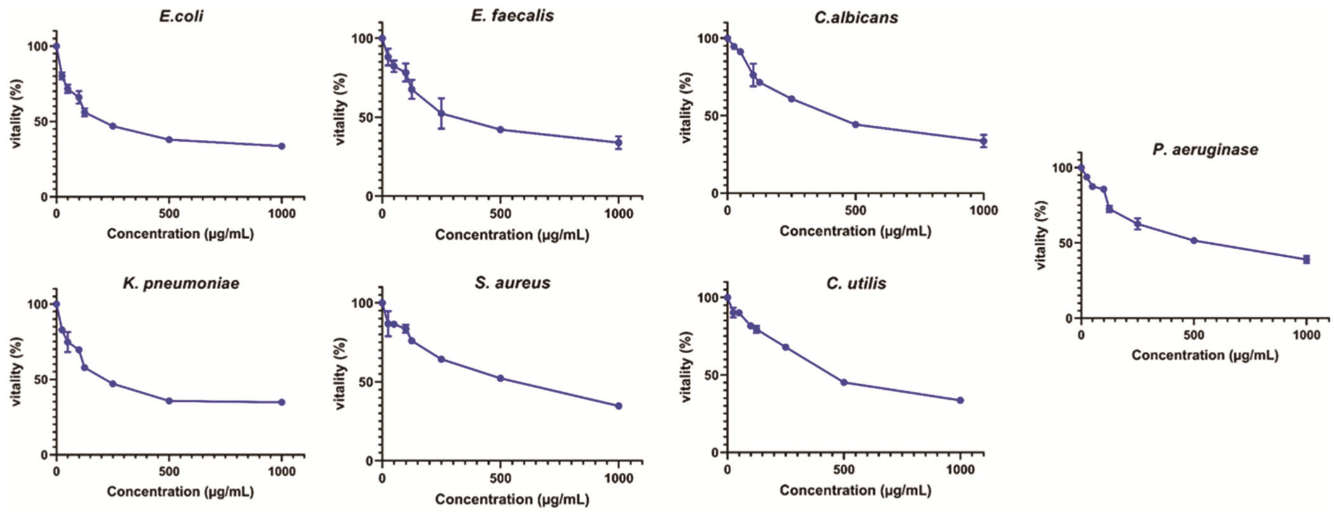


Fig. 8 ─ Viability graphs of pathogenic microorganisms exposed to NiO NPs (μg/mL)

of plasma membranes and cause to the death of cell which could not regulating the transitions in the membrane[62,63]. Besides, NPs penetrating the bacteria cell denature proteins by binding to functional groups on it [64].

## Conclusions

In brief, approximately 19-30 nm sized non-uniform NiO NPs were produced by calcination of the nickel-Schiff base complex for 4 h at 600°C. Morphology of the obtained NPs was investigated by FT-IR, UV-Vis, XRD, EDX and STEM methods. The results of the spectroscopic studies revealed that transformation of the Schiff base complex into NiO NPs was achieved with high purity by calcination method without using any special equipment or additive. This result proved the solid state thermal decomposition is cost-efficient and easy route for NiO NP formation and therefore the same method may be used to obtain other metal NPs from the same Schiff base precursor. The produced NPs were utilized as a photocatalyst for decomposition of MB in aqueous media of under sun-light irradiation and mild activity was observed by 49.31% decomposition rate. Besides, antibacterial properties of the NiO NP were investigated against five bacteria and two fungi. The NiO NPs, having dose dependent inhibitory effect on fungi, exhibited good antibacterial activity against five bacterial strains.

## References


1 Saghatforoush L A, Mehdizadeh R & Chalabian F, *Transit Met Chem*, 35 (2010) 903.
2 Wu J, Xia X, Guo R, Huang X & Lin Y, *Mater Res Bull*, 96 (2017) 315.
3 Kheradmandfard M, Minouei H, Tsvetkov N, Vayghan A K & Kashani-Bozorg S F, *Mater Chem Phys*, 262 (2021) 1.
4 Wang H, Wei W & Hu Y H, *Top Catal*, 57 (2014) 607.
5 Weber S, Rath T, Mangalam J, Kunert B & Coclite A M, *J Mater Sci Mater Electron*, 29 (2018) 1847.
6 Nalage S R, Chougule M A, Sen S & Patil VB, *J Mater Sci Mater Electron*, 24 (2013) 368.
7 Mokoena T P, Hillie K T, Swart H C, Leshabane N & Tshilongo J, *Mater Chem Phys*, 253 (2020) 1.
8 Suvith V S, Devu V S & Philip D, *Opt Quantum Electron*, 52 (2020) 1.
9 Rammal M B & Omanovic S, *Mater Chem Phys*, 255 (2020) 123570.
10 Vijaya Kumar P, Jafar Ahamed A & Karthikeyan M, *S N Appl Sci*, 1 (2019) 1.
11 Jabli M, Al-Ghamdi Y O, Sebeia N, Almalki S G & Alturaiki W, *Mater Chem Phys*, 249 (2020) 1.
12 Ezhilarasi A A, Vijaya J J, Kennedy L J & Kaviyarasu K, *Mater Chem Phys*, 241 (2020) 1.
13 Mousa S A, El-Sayed E S R, Mohamed S S, Abo El-Seoud M A & Elmehlawy A A, *Appl Microbiol Biotechnol*, 105 (2021) 741.
14 Anandan K & Rajendran V, *Mater Sci Semicond Process*, 14 (2011) 43.
15 Brewster D A, Bian Y & Knowles K E, *Chem Mater*, 32 (2020) 2004.
16 Chai H, Chen X, Jia D, Bao S & Zhou W, *Mater Res Bull*, 47 (2012) 3947.
17 Wu H, Wang Y, Zheng C, Zhu J & Wu G, *J Alloys Compd*, 685 (2016) 8.
18 Patel K N, Deshpande M P, Gujarati V P, Pandya S & Sathe V, *Mater Res Bull*, 106 (2018) 187.
19 Du Y, Wang W, Li X, Zhao J & Ma J, *Mater Lett*, 68 (2012) 168.
20 Wang Y & Su Q, *J Mater Sci Mater Electron*, 27 (2016) 4752.
21 Grivani G, Vakili M, Khalaji A D, Bruno G & Rudbari H A, *J Mol Struct*, 1072 (2014) 77.
22 Selvakumar R, Nirosha B, Vairam S, Premkumar T & Govindarajan S, *Inorganica Chim Acta*, 482 (2018) 774.

23 Goel S, Tomar A K, Sharma R K & Singh G, *ACS Appl Energy Mater*, 1 (2018) 1540.
24 Karthik K, Dhanuskodi S, Gobinath C, Prabukumar S & Sivaramakrishnan S, *J Mater Sci Mater Electron*, 29 (2018) 5459.
25 Alagiri M, Ponnusamy S & Muthamizhchelvan C, *J Mater Sci Mater Electron*, 23 (2012) 728.
26 Zhu Z, Bai Y, Zhang T, Liu Z & Long X, *Angew Chemie*, 126 (2014) 12779.
27 Salehirad A, *Russ J Appl Chem*, 89 (2016) 63.
28 Salavati-Niasari M, Mir N & Davar F, *J Alloys Compd*, 493 (2010) 163.
29 Khansari A, Enhessari M & Salavati-Niasari M, *J Clust Sci*, 24 (2013) 289.
30 Khalaji A D & Das D, *Int Nano Lett*, 4 (2014) 1.
31 Grivani G, Ghavami A, Eigner V, Dušek M & Khalaji A D, *Chinese Chem Lett*, 26 (2015) 779.
32 Khalaji A D, Grivani G & Izadi S, *J Therm Anal Calorim*, 126 (2016) 1105.
33 Salehi M, Galini M, Kubicki M & Khaleghian A, *Russ J Inorg Chem*, 64 (2019) 18.
34 Dehno Khalaji A, *J Clust Sci*, 24 (2013) 189.
35 Farhadi S, Kazem M & Siadatnasab F, *Polyhedron*, 30 (2011) 606.
36 Farhadi S & Roostaei-Zaniyani Z, *Polyhedron*, 30 (2011) 971.
37 Farhadi S & Roostaei-Zaniyani Z, *Polyhedron*, 30 (2011) 1244.
38 Samadi S, Khalili E & Allahgholi Ghasri M R, *J Electron Mater*, 48 (2019) 7836.
39 Motahari F, Mozdianfard M R & Salavati-Niasari M, *Process Saf Environ Prot*, 93 (2015) 282.
40 Kitchamsetti N, Ramteke M S, Rondiya S R, Mulani S R & Patil M S, *J Alloys Compd*, 855 (2021) 157337.
41 Wang G, Li Y & Zhuo S, *Int J Mater Res*, 101 (2010) 310.
42 Ramesh M, Rao M P C, Anandan S & Nagaraja H, *J Mater Res*, 33 (2018) 601.
43 Miri A, Mahabbati F, Najafidoust A, Miri M J & Sarani M, *Inorg Nano-Metal Chem*, 52 (2022) 122.
44 Fasina T M, Ogundele O, Ejiah F N & Dueke-Eze C U, *Int Juornal Biol Chem*, (2012) 24.
45 Brandt A L, Castillo A, Harris K B, Keeton J T & Hardin M D, *J Food Sci*, 75 (2010) M557.
46 Parvekar P, Palaskar J, Metgud S, Maria R & Dutta S, *Biomater Investig Dent*, 7 (2020) 105.
47 Khalaji A D, Jafari K & Rad S M, *Synth React Inorganic Met Nano-Metal Chem*, 45 (2015) 875.
48 Motahari F, Mozdianfard M R, Soofivand F & Salavati-Niasari M, *RSC Adv*, 4 (2014) 27654.
49 Hussain M M, Rahman M M & Asiri A M, *J Environ Sci (China)*, 53 (2017) 27.
50 Sheena P A, Priyanka K P, Sreedevi A & Varghese T, *J Nanostructure Chem*, 8 (2018) 207.
51 Siddique M N, Ahmed A, Ali T & Tripathi P, *AIP Conf Proc*, 1953 (2018).
52 Kalam A, Al-Sehemi A G, Al-Shihri A S, Du G & Ahmad T, *Mater Charact*, 68 (2012) 77.
53 Kawasaki S I, Sue K, Ookawara R, Wakashima Y & Suzuki A, *J Supercrit Fluids*, 54 (2010) 96.
54 Palanisamy P & Raichur A M, *Mater Sci Eng C*, 29 (2009) 199.
55 Zorkipli N N M, Kaus N H M & Mohamad A A, *Procedia Chem*, 19 (2016) 626.
56 Davar F, Fereshteh Z & Salavati-Niasari M, *J Alloys Compd*, 476 (2009) 797.
57 Chen Z, Xu A, Zhang Y & Gu N, *Curr Appl Phys*, 10 (2010) 967.
58 Khairnar S D & Shrivastava V S, *J Taibah Univ Sci*, 13 (2019) 1108.
59 Paul D & Neogi S, *Mater Res Express*, 6 (2019) 1.
60 Bhat S A, Zafar F, Mondal A H, Kareem A & Mirza A U, *J Iran Chem Soc*, 17 (2020) 215.
61 Al-Shawi S G, Alekhina N A, Aravindhan S, Thangavelu L & Kartamyshev N V, *J Nanostructures*, 11 (2021) 181.
62 Stoimenov P K, Klinger R L, Marchin G L & Klabunde K J, *Langmuir*, 18 (2002) 6679.
63 Chaudhary R G, Tanna J A, Gandhare N V, Rai A R & Juneja H D, *Adv Mater Lett*, 6 (2015) 990.
64 Khashan K S, Sulaiman G M, Ameer F A K A & Napolitano G, *Pak J Pharm Sci*, 29 (2016) 541.